sustainability

MDPI

Article

Bond Behavior of Recycled Tire Steel-Fiber-Reinforced Concrete and Basalt-Fiber-Reinforced Polymer Rebar after Prolonged Seawater Exposure

Fatemeh Soltanzadeh [1,*], Ali Edalat-Behbahani [1], Kasra Hosseinmostofi [1], Ibrahim Fatih Cengiz [2,3], Joaquim Miguel Oliveira [2,3] and Rui L. Reis [2,3]

1 Institute for Sustainability and Innovation in Structural Engineering (ISISE), Department of Civil Engineering, School of Engineering, University of Minho, 4800-058 Guimarães, Portugal; aliedalatbehbahani@gmail.com (A.E.-B.); id8645@alunos.uminho.pt (K.H.)

2 3B's Research Group, I3Bs-Research Institute on Biomaterials, Biodegradables and Biomimetics, University of Minho, Headquarters of the European Institute of Excellence on Tissue Engineering and Regenerative Medicine, AvePark, Parque de Ciência e Tecnologia, Zona Industrial da Gandra, Barco, 4805-017 Guimarães, Portugal; fatih.cengiz@i3bs.uminho.pt (I.F.C.); miguel.oliveira@i3bs.uminho.pt (J.M.O.); rgreis@i3bs.uminho.pt (R.L.R.)

3 ICVS/3B's-PT Government Associate Laboratory, 4806-909 Guimarães, Portugal

* Correspondence: f.soltanzadeh@civil.uminho.pt

Abstract: The integration of basalt-fiber-reinforced polymer (BFRP) rebars into concrete design standards still remains unrealized due to limited knowledge on the performance of the rebars in concrete, particularly in terms of bond durability in harsh conditions. In this work, we investigated the bond durability characteristics of BFRP rebars in fiber-reinforced self-compacting concrete (FRSCC) structures. To this aim, a number of 24 FRSCC pullout specimens reinforced with either BFRP rebar or glass-fiber-reinforced polymer, GFRP, rebar, which is a commonly used type of FRP, were fabricated. Half of these specimens were submerged in simulated seawater for a two-year span, while the other 12 similar specimens were maintained in standard laboratory conditions for comparative purposes. Subsequently, all 24 specimens underwent monotonic and fatigue pull-out tests. The exploration in this study focused on investigating the influence of the environmental condition, reinforcement type, and loading type on the bond stress versus slip relationship, maximum bond stress, and failure mode of the specimens. Based on the results obtained and by adopting the durability approach of industry standards for prediction of the bond retention of FRP-reinforced concrete, the bond strength retention between BFRP/GFRP and FRSCC after 50 years of exposure to seawater was estimated. The outcomes of the study are expected to enhance engineers' confidence in the use of FRP, especially BFRP, for constructing durable and sustainable reinforced concrete structures in aggressive environments.

Keywords: bond durability; bond strength retention prediction; basalt-fiber-reinforced polymer; hybrid RTSF/ISF-reinforced concrete; pullout test

check for updates

Citation: Soltanzadeh, F.; Edalat-Behbahani, A.; Hosseinmostofi, K.; Cengiz, I.F.; Oliveira, J.M.; Reis, R.L. Bond Behavior of Recycled Tire Steel-Fiber-Reinforced Concrete and Basalt-Fiber-Reinforced Polymer Rebar after Prolonged Seawater Exposure. *Sustainability* **2023**, *15*, 15856. https://doi.org/10.3390/su152215856

Academic Editor: Syed Minhaj Saleem Kazmi

Received: 10 October 2023
Revised: 31 October 2023
Accepted: 8 November 2023
Published: 11 November 2023

1. Introduction

Despite the inherent strength of concrete materials in harsh environments, the premature collapse of many reinforced concrete (RC) structures is attributed to the corrosion of steel reinforcement. Promising solutions for improving structural durability involve utilizing discrete fibers as either partial or complete shear reinforcement, adjusting based on steel fiber dosage, and employing fiber-reinforced polymer (FRP) as shear/flexural reinforcement [1–3]. Recycling end-of-life tires, ELTs, for steel fiber can enhance concrete sustainability in addition to providing longer service life for concrete structures. A recent study [1] found that compared to the industrial steel fiber, ISF, recycled tire steel fiber, RTSF, production emits fewer environmental pollutants, by reducing abiotic depletion potential (ADP) by up to 47% and global warming potential (GWP) up to 10%.

The application of FRP rebars as a substitute for steel flexural reinforcements is gaining prominence due to their advantages, including a high stiffness-to-weight ratio, fatigue resistance, easy handling, and resistance to corrosion [4]. The commonly used types of FRP bars are glass- and carbon-FRP rebars, with glass-FRP rebars being favored for their cost-effectiveness [5]. A relatively recent development is basalt-fiber-reinforced polymer (BFRP) rebars derived from volcanic rocks without additives, making them eco-friendly and non-hazardous material. Basalt fibers surpass E-glass in tensile strength and outperform carbon fibers in failure strain [6]. They also provide respectable resistance to chemicals, impact, and fire, all at a cost-effective price [7,8]. This makes BFRP rebars a rising choice for marine structures.

By means of employing both corrosion-resistant solutions, namely integrating discrete steel fibers and FRP reinforcements, it becomes possible to enhance structural ductility as compared to steel-reinforced concrete. This approach also improves the bond between concrete and FRP interfaces by surpassing plain concrete-reinforcement bonds. Recent research [9] indicated that replacing 50% of conventional ISF with RTSF in concrete production led to a 6.3% enhancement in FRP-concrete bond strength under static loading and a 10% improvement under a fatigue loading regime. RTSF's effectiveness stems from its greater fiber entanglement propensity, by means of creating a 3D network that bolsters the reinforcement–concrete bond.

The bond development between the FRP rebar and concrete is vital for the successful application of FRPs as reinforcement in concrete structures. This bond can significantly influence crack distribution, rebar anchorage, and structural serviceability of the concrete structure [10]. However, harsh environments such as seawater, water exposure, and wet-dry cycles can negatively change the performance of FRP-reinforced structural elements. For instance, a study on coral seawater sea-sand concrete beams reinforced with BFRP rebars showed an appropriate initial bending performance in normal conditions. However, under exposure conditions (6 h immersion in 40 °C artificial seawater followed by 6 h drying), cracks became sparse, shear resistance reduced due to BFRP stirrup degradation, and the failure mode changed from concrete crushing to shear failure as immersion time increased [11]. In marine conditions, corrosive ions such as Cl^- and $SO_4{}^{2-}$ from seawater penetrate the interior of the structures, corroding both the concrete and internal FRP rebars. The seawater permeates the concrete, creating a moist alkaline environment that causes localized damage to the resin matrix and fibers of the FRP rebars as well [12].

Ref. [13] examined the bond behavior of FRP rebars in concrete. This analysis encompasses both their immediate and extended (durability) characteristics. Based on an extensive database that includes data from 1002 pullout tests documented in the existing literature, they assert that while research on the bond between FRP rebars and concrete is growing, few studies address the long-term prediction of bond strength (known as bond strength durability). They suggested that "this gap in the literature is significant". To the best of the authors' knowledge, in most of the studies on assessment of the long-term bond behavior of FRP-reinforced structures [6,14,15], the accelerated aging studies are commonly preferred over real-time tests in labs due to the challenges of conducting long-term tests. These studies, carried out in controlled lab conditions, use heightened temperature, moisture, and stress to simulate accelerated deterioration [16], which often differ from actual field performance.

In the present study, we aim to address a knowledge gap by means of examining the bond behavior between BFRP and fiber-reinforced self-compacting concrete, FRSCC, after two years of immersion in seawater, without resorting to accelerated aging conditions. This research holds significant importance in the field as it collaborates with the application of novel materials and enhancing design methods for offshore structures, aiming to overcome the challenges posed by corrosion. It is part of a broader research project focused on developing corrosion-resistant offshore concrete structural elements. The reinforcing system in these structures is composed of FRP rebars and hybrid RTSF and ISF. Application of this reinforcing system can suppress the corrosion problems of steel-reinforced concrete structures by eliminating the steel stirrups using steel-fiber-reinforced self-compacting concrete, SFRSCC and by employing non-corrodible FRP longitudinal reinforcements. Moreover, the discrete fibers used in developing the FRSCC elements collaborate to overcome the shortcomings of FRP reinforcements in plain concrete structures by increasing the strength and stiffness and assuring the desired ductility. The RTSF reinforced concrete used in this study stems from extensive research aimed at optimizing the mechanical and environmental aspects of FRC. This study deliberately chose the best RFSF/ISF combination to ensure an effective FRP/concrete bond with minimal environmental impact. However, the limited understanding of the long-term performance of the applied materials hindered their widespread adoption. Therefore, this study specifically concentrates on characterizing the degradation of bond strength between FRP rebars and fiber-reinforced self-compacting concrete (FRSCC) after prolonged exposure to seawater. To the best of authors' knowledge, this study marks the first comprehensive exploration of the bond behavior between BFRP and RSF reinforced concrete, notably under fatigue loading conditions across a 50-year period from construction. What distinguishes this study is its dedication to exploring factors affecting BFRP's bond behavior, such as loading conditions, aging, and environmental impacts, particularly within the context of FRC offshore structures. Building upon prior research conducted by the authors regarding bond properties of BFRP-FRSCC at normal conditions [9], by considering factors such as reinforcement type (BFRP and GFRP), loading conditions (static and fatigue), fiber type for reinforcing the concrete (ISF and RTSF), and the direction of fiber-reinforced concrete flow in relation to rebar orientation, this study aims to provide a deeper understanding of BFRP-FRSCC bond durability after prolonged exposure to simulated seawater. Thus, this study addressed the following remaining queries: (*i*) to explore distinctions in the response of BFRP/GFRP-concrete bond pre/post seawater immersion; (*ii*) to identify whether the bond-slip behavior of FRSCC and BFRP, following extensive cycles of loading within an operational range of stress, varies notably from outcomes of static tests, after a long-term immersion in seawater and (*iii*) to examine the influence of type of reinforcement, i.e., BFRP or GFRP, with distinct surface features, on durability of the bond. Moreover, the study involved a theoretical prediction of the bond strength between FRSCC and BFRP reinforcement after 50 years of exposure to seawater. The calculated bond retention percentage after this extended service period holds both theoretical importance and practical relevance. The outcomes of this study will aid in the development of guidelines for effectively utilizing BFRP rebars in offshore structures.

This paper is presented in nine sections. Section 1 outlines the motivation and objectives, offering an overview of prior FRP rebar studies and addressing the lack of information and design guidelines for BFRP rebars in challenging conditions. In Section 2, we delved into the experimental program, covering aspects such as loading, rebar selection, aging techniques, and specimen conditioning. Section 3 introduces the materials used in the study, by providing essential information on their mechanical/physical properties. Section 4 explains the rationale behind the chosen aging method. Sections 5 and 6 detail specimen preparation and testing setup, respectively. Section 7 discusses the test results, while Section 8 predicts long-term bond strength. Finally, Section 9 concludes the research, and demonstrates areas that warrant further investigation in the realm of bond durability issues.

2. Experimental Program

A comprehensive examination of long-term FRP/FRSCC bond behavior immersed in seawater was conducted using a total of 24 bond specimens. The investigation also encompassed the analysis of the effect of the type of loading, i.e., static or fatigue loading type, and the type of adopted FRP rebar, i.e., basalt or glass FRP rebar, on this bond behavior. To this aim, the specimens were immersed in simulated seawater for a duration of 2 years, and their bond behavior was subsequently compared with unconditioned specimens.

3. Materials

3.1. Fiber-Reinforced Polymer Rebars

Herein, two types of reinforcements, namely BFRP rebar and GFRP reinforcements as commonly used types of FRP, with 12 mm diameter, were employed as depicted in Figure 1. The GFRP rebar features ribs on their surface, spaced at around 8.5 mm apart, with a fixed height that corresponds to 6% of the diameter of the rebar. The mechanical properties provided by the manufacturers were considered for both types of rebars, i.e., GFRP and BFRP. The GFRP rebar exhibited a reported tensile strength exceeding 1000 MPa and a modulus of elasticity of 60 GPa, whereas the sand coated BFRP rebar exhibited evident grooved helical spirals, with a spacing of 15 mm on its surface. The reported modulus of elasticity for this reinforcement was at least 60 GPa, with a minimum tensile strength of 1000 MPa.

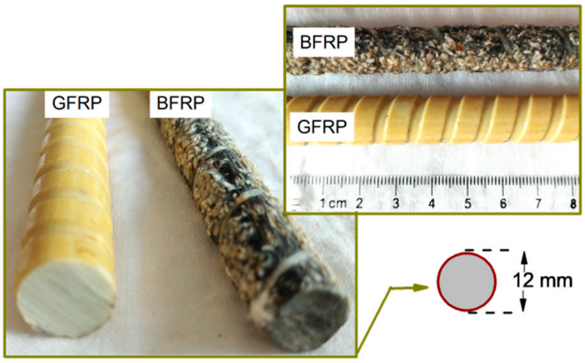

Figure 1. Fiber-reinforced polymer rebars adopted in this study.

3.2. Steel Fibers

Two types of steel fiber, specifically Recycled Tire Steel Fiber, RTSF, and Industrial Steel Fiber, ISF, were utilized to enhance the eco-efficiency and sustainability [1] of the applied concrete. Based on the results obtained in the previous studies [9], this study employed equal weight percentages of both recycled steel fibers and industrial steel fibers to reinforce the concrete. The objective was to enhance the bond strength between FRP and FRSCC compared to using a single type of fiber reinforcement.

The RTSFs were sourced from a scrap tire processing plant in Portugal, and the detailed process of recycling the steel fibers can be found in the work by Soltanzadeh et al. [1]. A visual representation of the RTSFs used in the present study, showing their varying diameters, lengths, and shapes is presented in Figure 2a. The mean diameter of the fibers, d_{Rf}, was determined to be 0.38 mm with a coefficient of variation (CoV) of 40%. The RTSF (Figure 2a) exhibited a mean length, l_{Rf}, of 33 mm with a CoV of 38%. The average fibers aspect ratio (l_{Rf}/d_{Rf}) was found to be 91 with a CoV of 40% and the average tensile strength of the RTSF was 1300 MPa. The typical surface characteristics of the fibers obtained via scanning electron microscopy (SEM) photomicrograph is illustrated in Figure 2b. This figure reveals predominantly smooth fibers, although some appear twisted, deformed, or partly shredded. In certain cases, rubber residue was observed to be attached to the fibers.

Figure 2c introduces the ISFs used for developing FRSCC, featuring a hooked-end shape and with the tensile strength of 1395 MPa. The fibers had a length, l_{If}, of 35 mm, a diameter, d_{If}, of 0.55 mm, and the aspect ratio (l_{If}/d_{If}) of the fibers was 64.

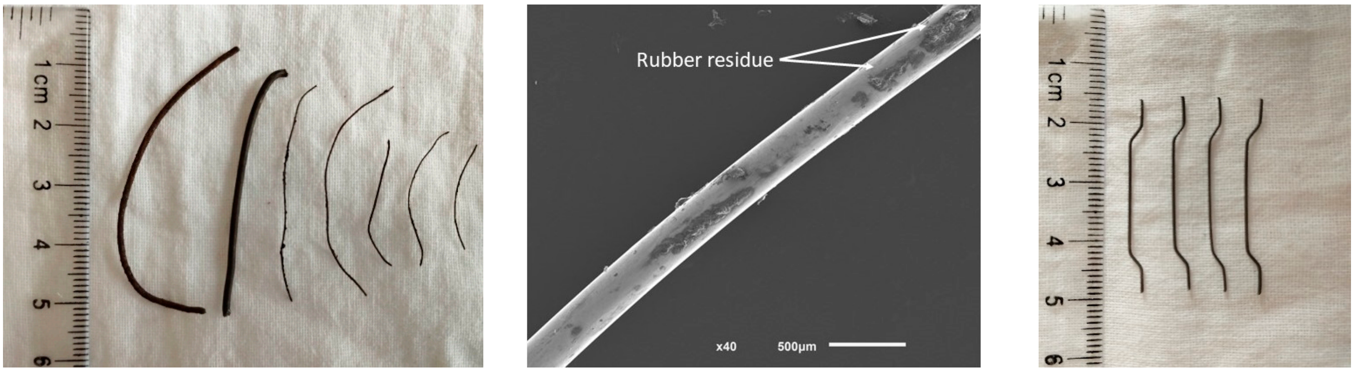

(**a**) (**b**) (**c**)

Figure 2. (**a**) Appearance of unsorted RTSFs, (**b**) surface characteristics of a RTSF, and (**c**) appearance of 35 mm length ISF.

3.3. Fiber-Reinforced Concrete

Based on the mix design methodology proposed by Soltanzadeh et al. [3], a self-compacting concrete reinforced with 90 kg/m^3 (corresponding to a volume fraction, Vf, of 1.15%) steel fibers was tailored in the present study for the fabrication of all the specimens. The formulation followed three critical steps: (i) optimizing material ratios for a bleed-free paste with ideal flowability and viscosity; (ii) determining the optimal volume percentages of each aggregate types for a densely packed SFRSCC, and (iii) assessing the optimum correlation between paste and solid skeleton to meet the desired maxi rheological and mechanical performance, aligned with the objectives of this study for constructing long-lasting prefabricated offshore structures. The adopted compositions for tailoring the FRSCC are introduced in Table 1. The concrete was produced using cement CEM I 52.5 R, fly ash, limestone filler, tap water, a second-generation of superplasticizer based on polycarboxylate ether (PCE) polymers (Glenium SKY 617), river sand with grain sizes of 0–2 mm, and crushed granite with grain sizes of 2–12.5 mm, and two types of steel fibers, i.e., RTSF and ISF. The adopted cement, CEM I 52.5 R, in developing the mix was recognized for its high early strength ("52.5" MPa at 28 days) and rapid strength development ("R"). Its use boosted paste free water content, thus improving workability through enhanced packing density. The limestone filler was adopted to create denser and more durable concrete. Additionally, spherical-shaped fly ash particles, acting as micro-rollers, effectively reduced friction and flow resistance in the paste. Detailed properties of these fine materials can be found in the authors' previous article [3]. Glenium SKY 617 superplasticizer was selected for developing the mix due to its remarkable capacity to enhance flowability while maintaining an appropriate paste viscosity. The aggregate dosage was carefully determined to ensure the mix achieved a compact skeleton while preserving its flowability. Based on the comprehensive evaluation of mechanical and environmental responses of several types of FRSCC in previous studies by the authors [1,9], the present research employed a promising approach by utilizing a hybrid combination of 45 kg/m^3 of ISF and 45 kg/m^3 of RTSF for reinforcing the concrete.

Table 1. Adopted material for tailoring the concrete reinforced by hybrid RTSF and ISF.

	C [1] (kg/m^3)	Fa [2] (kg/m^3)	Ls [3] (kg/m^3)	W [4] (L/m^3)	Sp [5] (L/m^3)	S [6] (kg/m^3)	Cs [7] (kg/m^3)	Ca [8] (kg/m^3)	ISF (kg/m^3)	RTSF (kg/m^3)
Compositions	504	200	151	231	18	107	568	435	45	45

[1] Cement; [2] fly ash; [3] limestone filler; [4] mixing water; [5] superplasticizer; [6] fine sand; [7] coarse sand (2 mm–4.75 mm); [8] coarse agg (4.75 mm–12.5 mm).

A proper rheological and mechanical properties were established in developing the FRSCC using the adopted mix design methodology. These properties were optimized specifically for the fabrication of precast prestressed offshore concrete elements, ensuring self-compacting behavior, high compressive and shear strength, and appropriate post-cracking residual strength. The FRSCC exhibited good homogeneity and cohesion during the slump test [17], with no visual signs of segregation. The fresh concrete achieved a spread diameter of 500 mm within 3.5 s (T50).

The 3D visualization of the hybrid recycled/industrial fiber orientation was conducted by employing micro-computed tomography (micro-CT) analysis. For this purpose, a concrete block measuring 570 × 570 mm^2 in the plane and 240 mm in thickness was cast from the center point, allowing for the fibers to be oriented perpendicular to the radial flow direction. After 28 days of casting, a sample of 50 × 50 × 120 mm^3 was drilled out of the concrete block. The specimen was polished using sandpaper to create smooth reflecting surfaces for performing the image analysis.

The specimen was scanned with the VivaCT 80 micro-CT system (Scanco Medical AG, Wangen-Brüttisellen, Switzerland), and the reconstructed 2D images were exported in TIF format with a pixel size of 26 µm using the manufacturer's software. The obtained images were then used for analysis and visualization by the software from Bruker (Bruker Micro-CT, Belgium). The steel fibers were scanned using the SkyScan 1272 micro-CT system (Bruker Micro-CT, Kontich, Belgium) at a pixel size of 5 µm. Then, the reconstruction of projections, analysis, and visualization were carried out using software from Bruker to generate a high-resolution image as shown in Figure 3a. The acquired data were utilized to determine the orientation of each fiber. By analysing the cut planes, it was possible to easily determine the orientation angle of the fibers. The orientations were defined in terms of Cartesian coordinates (Figure 3a), i.e., the fibers with an orientation angle of 90° were assigned to fibers oriented perpendicular to the XZ plane, i.e., concrete flow direction, and parallel to Y direction, whereas fibers parallel to the XY plane were assigned an orientation angle of 0°. The volume rendering image of fibers deviation from the vertical axis is shown in Figure 3b. Based on this image, 13.3% of the fibers were oriented within 0–30°, 26.1% within the range 30–60°, and 60.5% within the range 60–90°. The result suggested the appropriate flowability of the concrete mix since the number of RSF and ISF oriented vertically to the concrete flow direction is about 4.5 to 6.5 times larger than the number of fibers oriented parallelly.

The mechanical performance of the SFRSCC at the hardened state was evaluated by determining Young's modulus, E_{cm} [18], compressive strength, f_{cm} [19], and the flexural behavior [20] at the age of 28 days. The average E_{cm} was evaluated as 30.33 GPa (CoV = 1.22%) and the f_{cm} equal to 63.45 MPa (CoV = 1.03%) was obtained by testing the FRSCC, using three cylindrical specimens of 150 mm diameter and 300 mm height.

The post-cracking response of the FRSCC was investigated using three notched beams with a cross-section of 150 × 150 mm^2 and a length of 600 mm, following the guidelines outlined in the MC2010 [20]. The nominal values of the flexural properties of SFRSCC can be determined by analyzing the relationship between the applied force (F) and the crack mouth opening displacement, CMOD. The residual flexural tensile strengths, $f_{R,j}$, are evaluated based on the F-CMOD relationships as follows:

$$f_{R,j} = \frac{3}{2}\frac{F_j.l}{b.h_{sp}^2} \quad (1)$$

where F_j is the applied load corresponding to CMOD$_j$ (CMOD$_1$ = 0.5 mm, CMOD$_2$ = 1.5 mm, CMOD$_3$ = 2.5 mm, and CMOD$_4$ = 3.5 mm); l = effective span; b = width of the specimens, and h_{sp} = depth of the notched cross section.

The average residual flexural tensile stress parameters of SFRSCC are introduced in Table 2. The results showed that as the CMOD increased from 0.5 mm to 3.5 mm, there was a 29.5% reduction in the average residual flexural tensile stress of the tailored composition. Previous studies by the authors [9] have indicated that, in comparison to RSF, ISF demonstrated superior efficacy in enhancing the flexural capacity of concretes, accompanied by higher energy dissipation. The reason can be the shorter average length of

RTSF compared to ISFs, which reduces the capability of crack bridging for macro cracks. Moreover, the diverse shapes and entanglement potential of the RSFs can diminish the uniformity of fiber distribution. However, application of hybrid RSF/ISF can provide a better bond strength compared to using solely ISF for reinforcing the concrete.

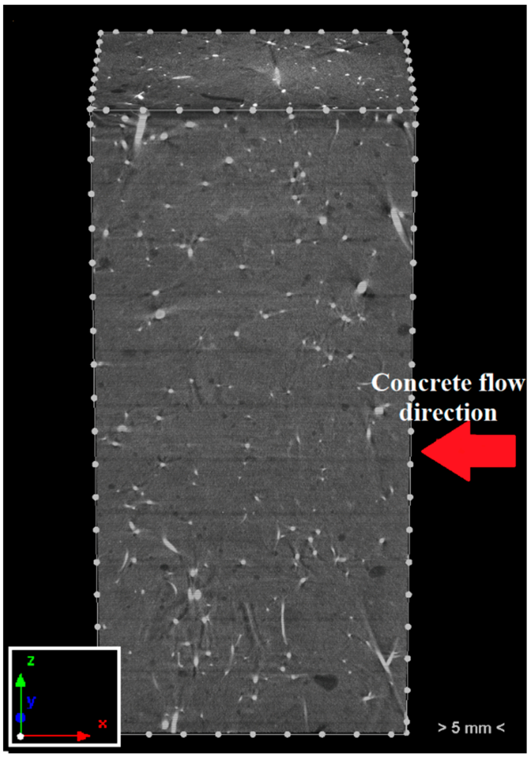

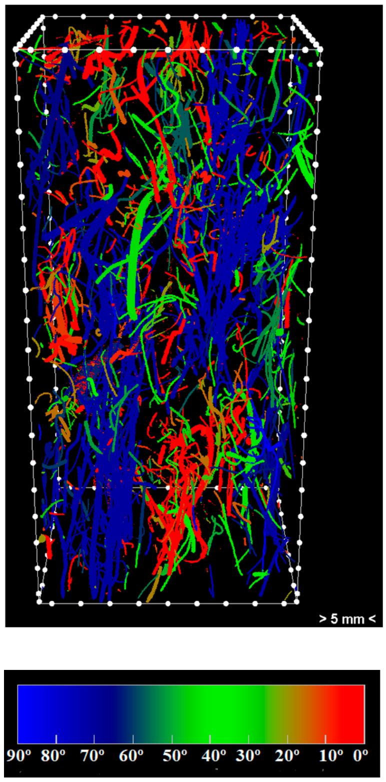

(a) (b)

Figure 3. (**a**) A 3D micro-CT image showing the general view of a specimen, and (**b**) 3D micro-CT image showing distribution of steel fibers in the same specimen.

Table 2. The residual flexural tensile strength parameters of SFRSCC.

	Residual Flexural Tensile Strength Parameters								**Limit of Proportionality** [1]		
	$CMOD_1$		**$CMOD_2$**		**$CMOD_3$**		**$CMOD_4$**				
	F_1 (kN)	**f_{R1} (MPa)**	**F_2 (kN)**	**f_{R2} (MPa)**	**F_3 (kN)**	**f_{R3} (MPa)**	**F_4 (kN)**	**f_{R4} (MPa)**	**F_L (kN)**	**$f_{ct,L}$ (MPa)**	**f_{Fst} [2] (MPa)**
Average	34.03	11.98	31.19	10.98	27.87	9.78	24.0	8.44	15.17	5.34	5.39
Cov (%)	9.07		3.82		3.30		2.82		5.10		

[1] Calculated by Equation (1) for CMOD = 0.05 mm; [2] this value is calculated as 0.45 f_{R1} according to MC2010.

4. Ageing Method

To evaluate the bond behavior of FRP rebars-FRSCC after prolonged exposure to an offshore environment, the natural aging method was selected in the present study as the most reliable approach [16] for testing. Incorporating the offshore environment's impact on rebar–concrete bond behavior in the literature often involves utilizing an accelerated method to artificially represent real-time aging. This process hinges on the temperature-aging rate relationship, where higher temperatures expedite the aging process. To provide accurate predictions of material durability through adopting the accelerated aging tests, a precise correlation must exist between the actual behavior of the material exposed to the real external environment for extended periods of time, and the experimental data obtained from accelerated aging tests. However, there are no established correlation factors that reliably relate the results of accelerated procedures to natural exposure to date. This is primarily due to several factors: variations in UV and solar spectral radiations, which differ in some way; the exposure parameters (such as temperatures, thermal variations, moisture levels, and UV-solar radiations) vary depending on the geographic location and season for outdoor exposure and can even fluctuate on a daily basis; moreover, complex interactions can occur between these different parameters [21].

As mentioned previously, this study forms part of a research initiative focused on developing high corrosion resistant concrete offshore elements. Based on the requirement of the project the environmental agents that have potential effects on the long-term structural behavior of the FRP/FRSCC system can be named as follows:

(i) Type of FRP rebars: FRPs are known for their enhanced durability in harsh marine environments compared to traditional steel reinforcements. However, they are not completely immune to degradation [22]. Exposure of FRP to seawater and alkaline environments can cause surface corrosion of the FRP rebars, which in turn raises concerns about the long-term bond between the FRP rebars and the concrete. Although the resin matrix provides some level of protection against degradation, continuous water diffusion into the resin can result in water absorption, hydrolysis, and subsequent degradation, plasticization, and swelling of the resin matrix. This process eventually leads to the occurrence of interfacial debonding between the fibers and the resin.

The long-term bond performance of FRP/FRSCC in a marine environment was evaluated in the present study by immersing the specimens in simulated seawater.

(ii) Humidity Effect: FRP rebars have a limited waterproofing property [23]. The moisture can permeate the resin and cause alterations to the mechanical characteristics and physical appearance of the material, such as an increase in volume. This can subsequently impact the overall performance of the bond between the FRP and FRSCC. The effect of humidity on FRP/FRSCC bond performance was automatically taken into account in the present study since the specimens were submerged in simulated seawater.

(iii) Alkaline Effect: FRP material undergoes degradation by exposure to alkaline substances due to a chemical reaction with the alkaline solution [24]. In the FRP-reinforced concretes, similar to the specimens developed in this study, FRP rods were incorporated within the concrete, which has a pH level as high as 13.5. In these specimens, the presence of an alkaline environment can harm the glass/basalt fibers by diminishing their toughness and strength. Embedment of the FRP rebars in FRSCC in the present study might have accelerated the potential degradation caused by alkaline without exaggerating (the possible degradation effect from alkaline). Thus, the test results are likely to be influenced by the mobility of alkaline ions.

5. Specimen Preparation and Conditioning

A number of 24 pullout specimens were prepared according to the recommendations of RILEM [25], by following two main criteria: (1) the lateral dimension of the cube specimen must be a minimum of 10 times the diameter of the rebar, and (2) the concrete cover should be at least five times the diameter of the rebar, d. In this study, the rebar diameter was 12 mm, so the side dimension of all specimens was set to 150 mm, which exceeds the required minimum of 120 mm. The rebars were centrally positioned within the concrete cube cross-section, maintaining a ratio of concrete cover (c) to rebar diameter (d) of 5.75. To maintain control over the length of the bond and mitigate inadvertent force transfer between the rebars and the FRSCC, the rebars were encased in plastic tubes with a diameter of 15 mm, except in the bond length region (as depicted in Figure 4). All specimens were cast using the same batch of FRSCC. Half of the specimens (a total of 12) were reinforced with BFRP rebars, while the remaining 12 specimens were reinforced with GFRPs.

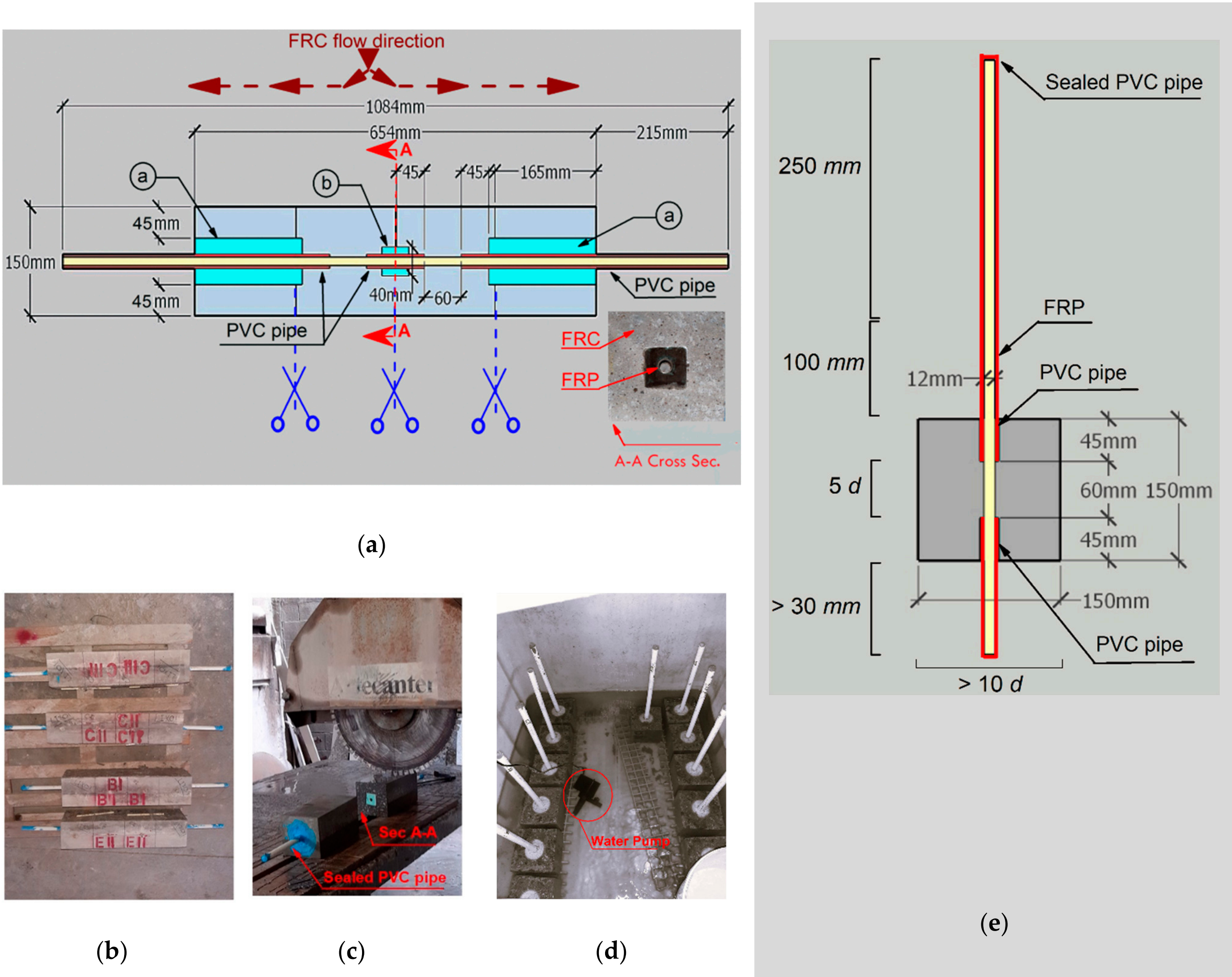

Figure 4. (**a**) Specimen preparation: (**a**) mold dimensions, (**b**) fabricated specimens, (**c**) cutting procedure (**d**) immerging specimens in seawater, and (**e**) details and dimensions of the pullout specimens.

As is already mentioned in Section 3.3, the orientation of the RTSFs is influenced by the direction of concrete flow. Therefore, the mold was specifically designed to facilitate the optimal fiber orientation, i.e., 0° angle with respect to FRP rebar direction, around the bond measurement area. The formwork was constructed with an internal length of 654 mm and uniform width and height of 150 mm as shown in Figure 4a,b. The rebar was placed along the length of the mold, resulting in fiber alignment parallel to the reinforcement (see Figure 4a). Once the specimens reached a curing time of 48 h, they were demolded (Figure 4b). Following a 7-day curing period, the specimens were divided into two sections along a plane perpendicular to the rebar axis. Each section was subsequently divided further to create a cube of 150 mm side dimension (see Figure 4c). To protect the reinforcement rebar from damage, two pieces of PVC tubes (labeled as “a” in Figure 4a) with a diameter of 60 mm were placed at the ends of the reinforcement. To replicate accurately the real conditions, the unbonded FRP regions, i.e., the free end and loaded end of the specimens, were safeguarded by encasing them in PVC pipes and sealing them with waterproof epoxy. It protected the FRP reinforcement (without concrete cover) from direct saltwater exposure. Moreover, a cubic foam component (identified as “b” in Figure 4a) of 40 mm side dimension was positioned at the center of the mold. This foam was later removed to create space for installing a Linear Variable Differential Transformer (LVDT) at the free end of the reinforcement (refer to the A-A cross section in Figure 4a).

After 28 days of casting, 12 specimens, consisting of 6 reinforced with BFRP and 6 reinforced with GFRP, were submerged in simulated seawater inside plastic containers adopted for the study (Figure 4d). The seawater was simulated using 24.53 g NaCl, 5.20 g $MgCl_2$, 4.09 g Na_2SO_4, and 1.16 g $CaCl_2$ in 1 L deionized water, as per ASTM D1141-98 [26]. Both the specimens and the container were kept at 23 °C for 24 months of conditioning. The container was covered with polyethylene sheeting to avoid water evaporation during conditioning. Furthermore, the water level was kept constant throughout the study to avoid a pH increase that could result from decreased water level and a significant increase in alkaline ions in the solution. The simulated seawater compositions were circulated every 3 h using an electric water pump. The specimens were removed from the alkaline solution after a duration of 24 months. Prior to testing the specimens, the PVC pipes and epoxy were removed from the FRP rebars to prevent undesired mechanical anchoring effects and preserve the bond behavior during the pull-out test. The specimens were subsequently tested using an identical test setup by means of employing either a static or fatigue loading regime.

Table 3 presents a comprehensive summary of the tested specimens and studied variables. The labelling method used for specimen designation follows a specific convention: The first letter, either 'G' or 'B', denotes the type of rebar utilized (BFRP or GFRP), while the second letter 'W' or 'D' signifies whether the specimen was subjected to immersion in seawater or not, and finally, the third character, "S" or "F" designates the condition of loading, specifically static (S) or fatigue (F) loading.

Table 3. Specifications of the tested specimens in the present study.

Specimen ID	FRP Type (B/G)	Loading Condition (S/F)	Environmental Condition (W/D)	Number of Specimens
B-D-S	BFRP	Static	Unconditioned	3
B-W-S	BFRP	Static	Conditioned	3
B-D-F	BFRP	Fatigue	Unconditioned	3
B-W-F	BFRP	Fatigue	Conditioned	3
G-D-S	GFRP	Static	Unconditioned	3
G-W-S	GFRP	Static	Conditioned	3
G-D-F	GFRP	Fatigue	Unconditioned	3
G-W-F	GFRP	Fatigue	Conditioned	3

6. Test Setup and Loading Procedures

The pull-out test was conducted, based on RILEM recommendation [25], using the test setup shown in Figure 5. The adopted test setup implemented optimization outlined by Chu and Kwan [27] to minimize pressure at the interface between the concrete cube and the steel plate in the testing setup. The pull-out samples were positioned on the setup, with the steel tube (refer to No. 4 in Figure 5) securely clamped (No. 8 in Figure 5) to the loading end of the actuator. A thick steel plate with a central hole facilitated the passage of the reinforcing rebar while providing support to the concrete face near the loaded end of the rebar (No. 7 in Figure 5). The diameter of the hole was adopted as 70 mm based on the recommendation of Chu and Kwan [27] A sulfur capping layer of 3 mm in thickness was carefully used to cover the upper surface of the concrete blocks in order to rectify the surfaces in contact. This layer ensured a smoother interface between the concrete and steel surfaces. A 1.5 mm thick low-friction polytetrafluoroethylene (PTFE) film, with a coefficient of friction of 0.05 (No.6 in Figure 5), was utilized in conjunction with the steel (No. 7 in Figure 5) to facilitate sliding between these surfaces. This combination allowed for easy movement and reduced the constraint of the steel plate on the concrete's lateral expansion. Moreover, a coating of grease was employed between the stainless-steel plate and the PTFE film to further diminish friction. This additional lubrication ensured smoother sliding motion and enhanced the overall performance of the setup.

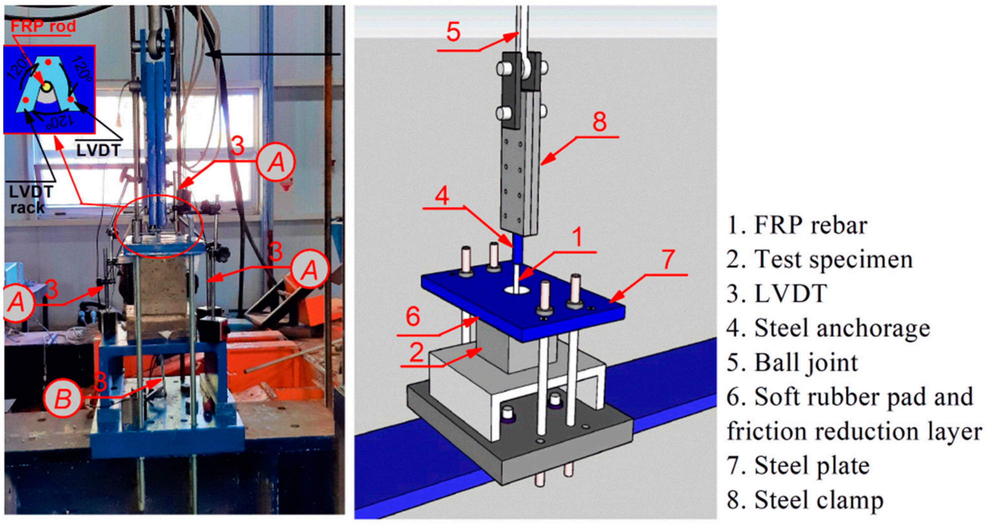

Figure 5. Adopted pull-out test setup in the present study.

A ball joint (No. 5 in Figure 5) was incorporated at the upper end of the test setup to prevent the FRP from bending due to misalignment. The relative displacement between the FRP rebar and the FRSCC at the loading end (labeled as 'A' in Figure 5) was directly measured by averaging the displacements recorded using three LVDTs installed at 120° intervals around the FRP rebar on a rack. These LVDTs were utilized instead of relying on the displacement recording system of the testing machine to exclude any influence from the deformation of the test setup. Moreover, the relative displacement between the rebar and the concrete surface was monitored using an additional LVDT, placed at the free end of the rebar (labeled as 'B' in Figure 5).

The 12 unconditioned specimens, also referred to as the control specimens, were subjected to testing after 28 days of casting. The 12 remaining specimens were tested at the termination of a 28-day curing period followed by an additional conditioning period of 24 months. A universal testing machine with a maximum load capacity of 200 kN was used to apply the static pull-out load. Throughout all static tests, the testing machine head implemented displacement control, which was operated at a predetermined displacement rate of 0.021 mm/s. This allowed us to observe the bond–slip relationship after reaching the peak load. Instrument data were recorded at a rate of 2 Hz using an acquisition system.

The fatigue tests were carried out under load control with a specified target of 10^6 cycles, in accordance with the recommendation of Wang and Belarbi [28]. After reaching the targeted number of cycles, the surviving specimens underwent static pull-out loading until failure occurred.

In order to conduct the fatigue test, the authors referenced their previous research [9] which determined the appropriate load intervals for testing BFRP reinforce FRSCC specimens under fatigue loading. This investigation was necessary due to the absence of established guidelines or specific recommendations for fatigue strength testing of BFRP rebars. Generally, the fatigue strength of FRP rebars is considerably lower than their static ultimate strength (f_{tu}). To prevent premature fracture of the reinforcement during fatigue testing, it is crucial to apply only a fraction of f_{tu}. On the basis of the authors' previous research, a stress range of 15–30% of the maximum bond stress, $\tau_{\max}$ (hereafter referred to as bond strength), was adopted for the fatigue test.

Based on the applied pull-out force, P, the bond stress τ is determined by assuming a uniform distribution of bond stress along the embedment length of the rebar, as follows:

$$\tau = \frac{P}{\pi d L} \quad (2)$$

where L is embedment length of the rebar.

7. Results and Discussion

In this section, a comprehensive examination of the findings was presented. The discussion has been structured into distinct subsections, each dedicated to a specific aspect of the investigation. First, the effects of aging on the physical appearance of concrete specimens were introduced in Section 7.1. Moving on to Section 7.2, the pullout response of the FRSCC specimens, reinforced with BFRP rebars, was evaluated and compared with specimens reinforced with GFRP, a commonly used FRP material. In Section 7.3, differences in bond behavior of the specimens when subjected to various loading regimes, including quasi-static and fatigue loading, are explored. The environmental conditioning effect on bond behavior is detailed in Section 7.4. Finally, the analysis is concluded in Section 7.5 by discussing the failure modes observed in all tested specimens.

7.1. Appearance of Concrete Specimen after Environmental Conditioning

After a 24-month exposure to seawater, all FRSCC specimens displayed structural integrity, as depicted in Figure 6a. Some steel fibers on the surface of the specimens exhibited corrosion products. However, the resulting damage was confined solely to the surface and could be readily eliminated by sanding the affected areas of the specimens, as depicted in Figure 6b.

(**a**) (**b**)

Figure 6. (**a**) Appearance of BFRP/GFRP-reinforced FRSCC specimens after 24 months of exposure to simulated seawater, and (**b**) surface of a specimen before and after surface sanding.

Evaluating of the corrosion susceptibility of RSF and ISF and its impact on the post-cracking behavior of SFRC in a corrosive environment [29] has revealed that RSF experiences generalized surface corrosion, indicating a slightly higher susceptibility to corrosion compared to ISF. Nevertheless, concrete reinforced with either hybrid or mono ISF/RSF offers good resistance to corrosion-induced strength loss, with corrosion typically penetrating no more than 1 to 3 mm into the concrete.

7.2. Effect of the Type of FRP Reinforcement

The average values of the obtained bond strength, Av. $\tau_{\max}$, and its corresponding slip at the free end, as well as the design bond strength, τ_{Design}, are represented in Table 4. In this study, the average of $\tau_{\max}$, for each series of specimens was evaluated as the maximum pullout, $P_{\max}$, force over the embedded area of the rebar, i.e., $\tau = \frac{P_{\max}}{\pi d L}$, whereas the bond strength corresponding to 0.05 mm slippage at the free end was adopted as the τ_{Design}.

Table 4. Results of pullout tests conducted under either monotonic or fatigue loading conditions.

Specimen ID	Av. $\tau_{\max}$ (MPa)	Av. $S_{\max}$ (mm)	Av. τ_{Design} (MPa)	Mode of Failure		
				SP. No. 1	SP. No. 2	SP. No. 3
B-D-S CoV (%)	27.39	2.06	8.61	Concrete splitting	Slip	Slip
B-W-S CoV	12.14	3.80	4.00	Slip	Slip	Slip
B-D-F CoV (%)	27.30	2.94	6.50	Concrete splitting	Concrete splitting	Concrete splitting
B-W-F CoV (%)	13.90	3.24	4.60	Slip	Slip	Slip
G-D-S CoV (%)	23.50	0.50	6.50	Slip	Slip	Slip
G-W-S CoV (%)	22.46	0.98	12.74	Concrete splitting	Slip	Slip
G-D-F CoV (%)	24.16	1.62	1.40	Concrete splitting	Concrete splitting	Slip
G-W-F CoV (%)	25.78	1.50	11.15	Concrete splitting	Concrete splitting	Slip

The typical bond-slip responses of BFRP- and GFRP-reinforced concrete at the free end before long-term immersion in seawater is depicted in Figure 7a. Upon comparing the bond-stress responses of BFRP -reinforced specimens (B-D-S) and GFRP-reinforced specimens (G-D-S) prior to immersion in seawater, i.e., the control specimens, it becomes evident that in both types of specimens, the bond stress was primarily influenced by the chemical bonding of the FRP rebars to the concrete. In this phase of the test, no notable differences were detected between the two-specimen series, indicating a similar level of chemical adhesion between the concrete and the respective rebars, was detected. However, once the chemical adhesion between the concrete and reinforcement was disrupted in the initial loading stage, the BFRP rebars demonstrated a higher bond stress during the rest of the pullout test.

By loading specimens reinforced using GFRP rebars, once the adhesive bond was surpassed, force transfer relied on the force developed by interlocking the ribs of the rebar with FRSCC, leading to an increased bond strength of up to Av. $\tau_{\max}$ = 23.5 MPa. During this stage, both the rebar and concrete suffered combined damage, with internal cracks initiating and propagating within the concrete substrate and rebar ribs. Consequently, the surface layer of the GFRP rebar peeled off. The bond stress achieved at this point was primarily dependent on the strength of the underlying concrete. Ultimately, failure took place at a critical point between consecutive fiber layers of the GFRP rebar, where the cohesive adhesion between fibers and resin governed the post-peak bond capacity of the tested specimens.

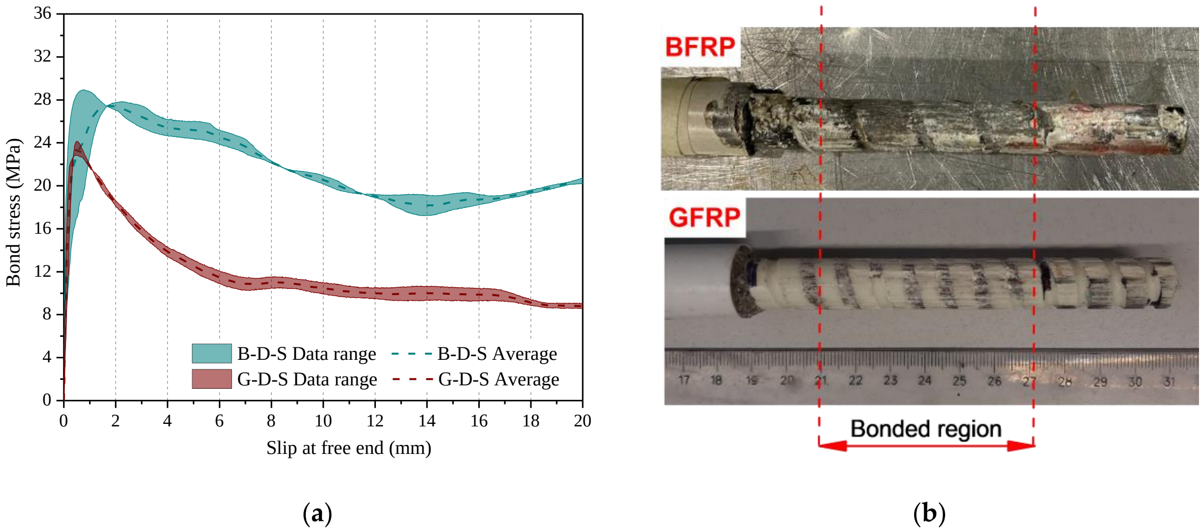

Figure 7. **(a)** Comparison of average τ-s response of BFRP-reinforced specimens with that of GFRP-reinforced specimens at normal condition, and (**b**) the condition of the rebars after testing the specimens.

For the BFRP-reinforced specimens, the bond-slip response closely resembled that of the GFRP specimens up until approximately Av. τ = 23.5 MPa. However, beyond this point, the unique surface characteristics of the BFRP, with its helical wrapping coated in sand, caused destruction along multiple orientation planes. As a result, the dominant peeling action on the rebar surface (found in the instances of the specimens reinforced by GFRP rebars) was not observed, and the cracking process within the surrounding concrete played a more significant role in governing the BFRP-concrete bond behavior. The presence of fibers effectively bridging the concrete cracks not only restrained the propagation of cracks but also significantly enhanced both peak loads, P_{max}, and maximum bond strength, τ_{max}. The average value of τ_{max} reached to 27.5 MPa, suggesting the positive impact of BFRP rebar on reinforcing the concrete. Comparatively, when employing BFRP rebars instead of GFRP rebars, there was a notable 17% increase in Av. τ_{max}, highlighting the superior performance of BFRP in this regard.

The behavior of the bond during the post-peak phase was controlled by two factors: (i) the fiber bridging effect, which limited the spreading of shear cracks, and (ii) the deterioration of the rebar's rough surface. At approximately Av. τ = 18.14 MPa, corresponding to a slip of 14 mm, the pre-existing cracks were substantially widened, allowing the fibers to solely transmit residual stresses. Compared to the BFPR-reinforced specimens, the G-D-S specimens exhibited a reduction of 51% in residual bond stress (Av. τ = 8.83 MPa) at a free end slip of approximately 20 mm. This reduction in stress indicated the diminished performance of the GFRP in resisting further slip and load transfer.

The intact BFRP ribbed surface, causing friction through wedging action, initiated a second stiffening stage [30]. This resulted in a second peak force for pull-out, corresponding to Av. τ = 20.50 MPa at a slip of around 20 mm.

After completing the tests, the results revealed notable differences in the surface defects that occurred in the BFRP and GFRP rebars during the pull-out test. In the case of the specimens reinforced with BFRP rebar, the rebar's surface with sand-coated treatment experienced significant rubbing and scratching, causing the resin to wear off. However, despite this damage, the general appearance of the rebar remained unchanged, and the grooved helical spirals were still observable, as illustrated in Figure 7b. On the other hand, the GFRP showed partial damage to the rebar surface, as depicted in Figure 7b. The rubbing action caused the resin to be eroded from the GFRP surface, while the concrete was pressed against the rebar deformations. Additionally, the detached resin scale was detected on the concrete specimen. Nonetheless, similar to the BFRP case, the fundamental structure of the GFRP rebar was unaffected.

7.3. Effect of Loading Regime

Figure 8 presents a comparison of bond-slip relationships for four specimen series: two reinforced with BFRP and the other two reinforced with GFRP rebars. The first pair of comparisons involves the bond behavior of BFRP-reinforced specimens subjected to quasi-static loading (B-D-S) with that of the specimens subjected to fatigue loading (B-D-F), as illustrated in Figure 8a. Similarly, Figure 8b compares the response of GFRP-reinforced specimens under quasi-static pullout loading (G-D-S) with those under fatigue loading regime (G-D-F).

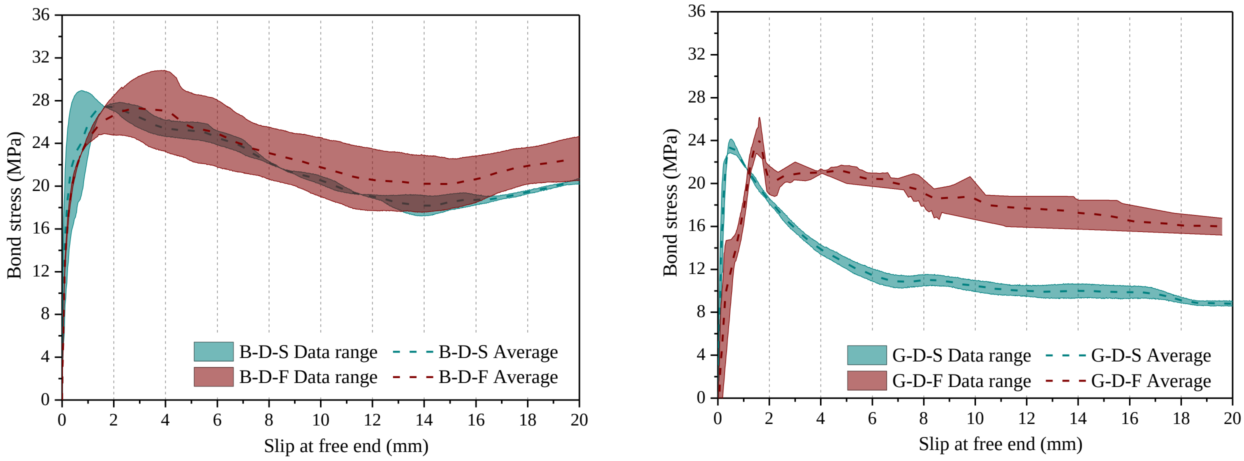

(**a**) (**b**)

Figure 8. Bond stress versus slip relationship derived from testing the specimens reinforced with (**a**) BFRP and (**b**) GFRP, under static and fatigue loading.

Overall, the findings indicate that fatigue loading appears to enhance the bond stiffness between FRP and concrete. This is evident from the higher bond stress observed at nearly all free end slip levels when comparing the responses of fatigue-loaded specimens to those subjected to quasi-static loading. Specifically, by testing the BFPR-reinforced specimens under fatigue loading there is a slight increase of 10% in the residual bond stress, and the obtained $\tau_{\max}$ and τ_{Design} results were almost equal to those obtained by considering the specimens tested under quasi-static loading. In comparison to the bond response of BFRP-reinforced specimens, the specimens reinforced with GFRP rebar demonstrated even greater enhancement under fatigue loading. Notably, fatigue loading substantially improved the post-peak bond response, with a 45% improvement in the residual bond stress corresponding to 20 mm free end slip, when compared to quasi-static loading results.

The improvement in bond behavior of the tested specimens can be attributed to fatigue loading. In general, during the casting of reinforced concrete elements, the rebar and concrete typically do not achieve full contact, as there remain some micro-voids between them. Additionally, application of the steel fibers for reinforcing the concrete causes a perturbation effect that provides additional micro-voids and matrix defects. Loading the specimen under fatigue loading regime led to the closure of some of these voids, resulting in a larger contact area and increased stiffness. Furthermore, fatigue loading roughens the rebar surface, significantly, and enhances the frictional resistance. These observations align with previous studies conducted by Wang and Belarbi [28] as well.

7.4. Environmental Conditioning Effect on Bond Behavior

After 24 months of exposure of specimens to the simulated seawater, BFRP-reinforced specimens exhibited a comparable behavior path within the control specimens in the same testing group (compare Figures 8a and 9). However, prolonged exposure to seawater caused a severe weakening of the bond-slip, τ-s, response of BFRP-reinforced specimens, as illustrated in Figure 9. In this figure, the bond stress versus slip curve of all the conditioned and unconditioned specimens reinforced with BFRP, and loaded under either quasi-ecstatic or fatigue regime, displays slight ascending and descending branches. The presence of these branches can be attributed to the limited development of cracks developed during the testing. At the peak, a slight decrease in bond stress is evident, but it quickly rebounds and rises to a second peak, resulting in a distinctive wave-like pattern of residual bond stress. The appearance of this wave-like shape in the bond stress versus slip curve is likely due to the complex interactions between the BFRP rebar and the surrounding concrete. The behavior can be attributed to various factors, including frictional effects and local variations in the bond conditions. A similar wave-like pattern in the τ-s curve was also noticed in research conducted by Lei et al. [31]. Their study focused on the bond properties between CFRP rebars and coral concrete in seawater environments at various temperatures (30, 60, and 80 °C). Their findings proposed that prolonged immersion and higher temperatures can lead to an elevation in such characteristic wave-like pattern τ-s curves.

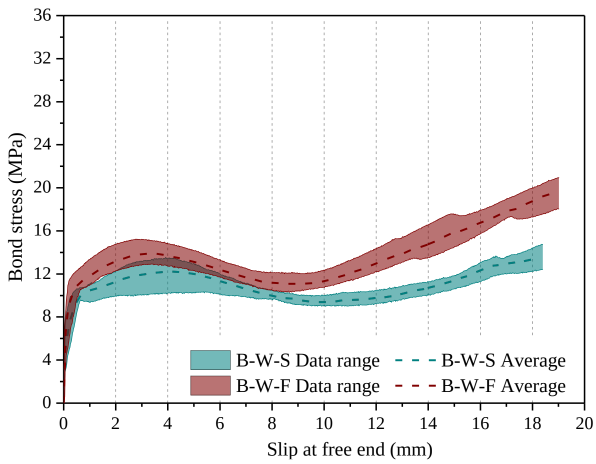

Figure 9. Comparison of the bond response of BFRP reinforced specimens tested under static loading conditions versus those tested under fatigue loading after immersion in simulated seawater.

Figure 10 demonstrates the significant impact of immersion in seawater on the bond strength of BFRP-reinforced specimens, i.e., B-W-S, and B-W-F. Compared to the unconditioned specimens tested under quasi-static loading, B-D-S, a reduction of 55.7% and 53.5% was observed in the maximum and designed bond strength of the conditioned specimens, respectively, i.e., B-W-S, following the long-term immersion. The same comparison can be made by considering the bond response of unconditioned BFRP-reinforced specimens with the conditioned ones, after passing one million cycles of loading (Figure 10b). The long-term immersion of B-W-F specimens in seawater, led to a reduction in $\tau_{\max}$ and τ_{Design} by 49% and 29%, respectively, in comparison with those of the B-D-F specimens. Compared to unconditioned specimens, the residual bond strength of the conditioned BFRP-reinforced specimens, corresponding to 20 mm free end slip, was reduced by 33.5% and 18.8% under quasi-static and fatigue loading, respectively.

The weakening of bond-slip curves in the case of the BFRP-reinforced specimens can be attributed to the moisture absorption in BFRP [32]. The FRP rebars do not possess inherent waterproofing properties, allowing moisture to permeate the polymer resin to some extent. The presence of water molecules can act as resin plasticizers, potentially resulting in the degradation of the polymer resins by disrupting van der Waals bonds within the polymer chains. It leads to the de-bonding of the resin matrix from the surface of the fibers of the rebar.

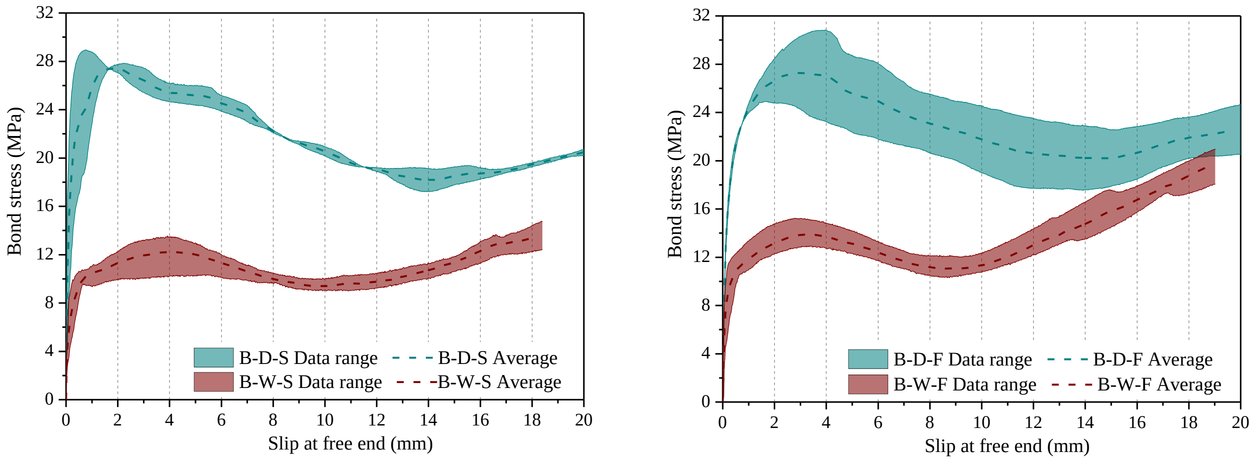

(**a**) (**b**)

Figure 10. Free-end bond-slip response of conditioned versus unconditioned BFRP-reinforced specimens, subjected to (**a**) quasi-static and (**b**) fatigue pullout loading.

In contrast to BFRP-reinforced concrete, conditioned specimens reinforced with GFRP exhibited an almost similar Av. τ_{max} to the corresponding control specimens, as shown in Figure 11. The improvement of the concrete compressive strength by immersion of the specimens in seawater led to an improvement in residual bond strength under both quasi-static and fatigue loading regimes. Specifically, the long-term immersing the GFRP-reinforced specimens in seawater resulted in an improvement of 21.7% and 32.5% in residual bond strength at 20 mm free end slip for those loaded under quasi-static and fatigue regimes, respectively.

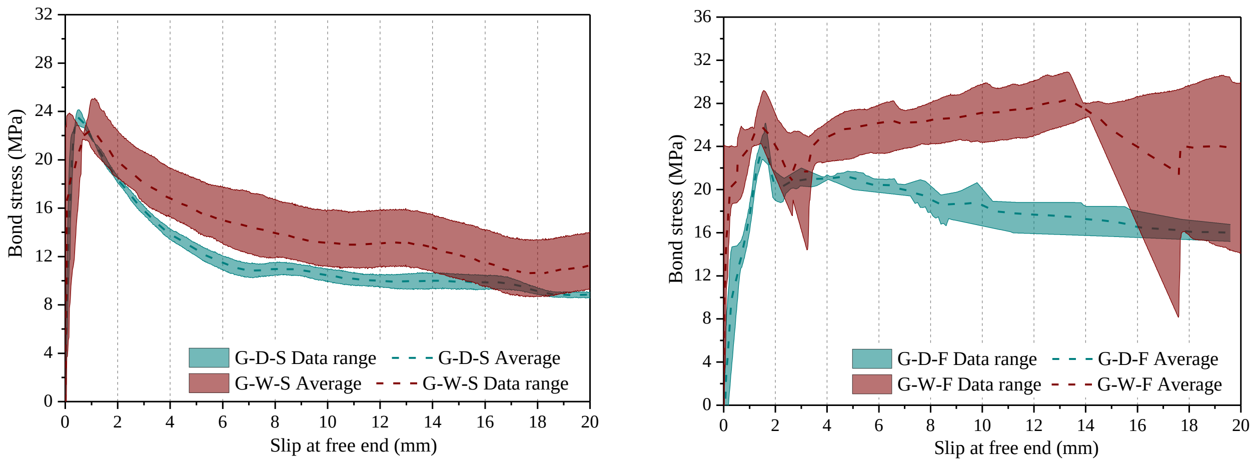

(**a**) (**b**)

Figure 11. Free-end bond-slip response of conditioned versus unconditioned GFRP-reinforced specimens, subjected to (**a**) quasi-static and (**b**) fatigue pullout loading.

A significant scatter becomes evident after a slip of 14 mm in the GFRP rebar of G-W-F specimens, as shown in Figure 11b. This scatter is attributed to an abrupt descending branch observed in the bond stress–slip curve of two out of the three conditioned specimens, i.e., G-W-F. The probable cause for this abrupt descent was the rapid development of splitting cracks that extended to the edge of the concrete specimen in a short time. As a result, there was a sudden decrease in bond stress, which could be clearly observed. However, the specimen was not broken into parts entirely, and the surrounding concrete continued to exert a constraint effect on the GFRP rebar. As a result, the bond stress gradually increased, but it could not reach the level before the split due to energy release. It is worth noting that the concrete's constraint effect was limited. The increase in slip under the pullout force was accompanied by further deterioration caused by the concrete split, leading to a gradual decrease in bond stress.

In this study, the BFRP-reinforced specimens exposed in a long-term seawater immersion, i.e., respectively B-W-S, B-W-F, suffered the most serious degradation of the bond between rebars and FRSCC (respectively with Av. τ_{max} equal to 12.14 MPa and 13.90 MPa), followed by the respectively conditioned and unconditioned specimens with GFRP reinforcement, i.e., respectively G-W-F (Av. τ_{max} = 13.90 MPa), G-W-S (Av. τ_{max} = 22.46 MPa), G-D-S (Av. τ_{max} = 23.50 MPa), G-D-F (Av. τ_{max} = 24.16 MPa), and finally the unconditioned BFRP-reinforced specimens, i.e., respectively B-D-F, and B-D-S (with Av. τ_{max} equal to 27.30 MPa and 27.39 MPa, respectively). In fact, when comparing the bond stress–slip relationship of specimens reinforced by GFRP rebars with those of BFRP-reinforced specimens, the latter exhibited a greater reduction across all loading stages in both static (Figure 12a) and fatigue (Figure 13a) loading conditions. This phenomenon proves the superior durability of GFRP rather than BFRP in seawater, which aligns with the results reported by Wang et al. [33].

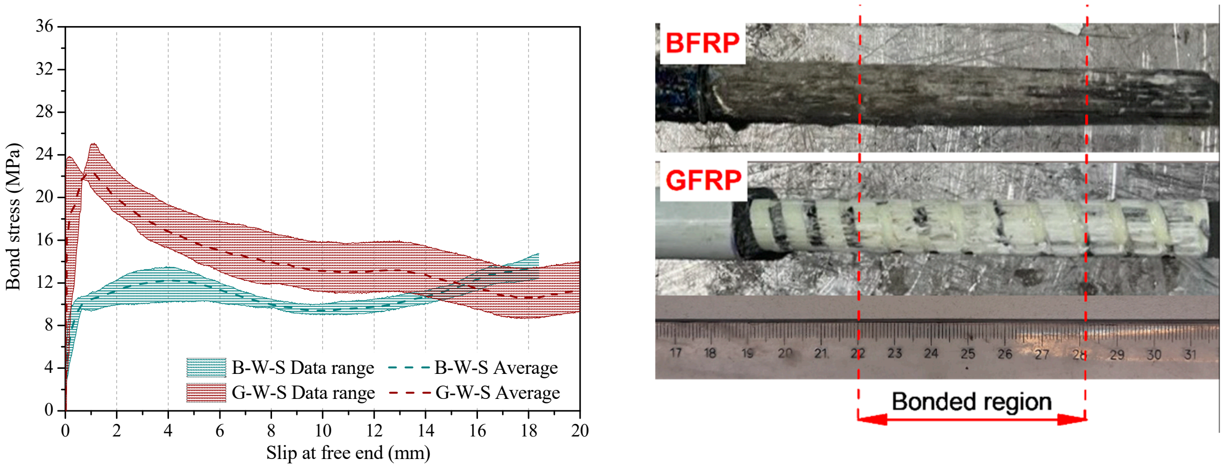

(**a**) (**b**)

Figure 12. **(a)** Bond behavior of BFRP-reinforced specimens versus that of GFRP-reinforced specimens immersed in simulated seawater, under static loading regime, and (**b**) condition of the rebars after performing the test.

Comparing the surface condition of the BFRP/GFRP illustrated in Figures 7b and 12b, it becomes evident that the extent of bond degradation varied for specimens exposed to different environmental conditions. In the case of the unconditioned BFRP/GFRP-reinforced specimens (control specimens), the failure interfaces were partially on the FRSCC and partially on the ribs of the FRP rebars. However, when the BFRP-reinforced specimens were immersed in seawater, the damage to the ribs increased significantly as the failure interface approached the core of the rebar, resulting in bond degradation. The specimens under seawater immersion experienced a severe degradation in bond performance between BFRP rebars and FRSCC, and the grooved helical spirals and the sand-coated surface treatment disappeared completely, while the unconditioned BFRP-reinforced specimens exhibited relatively less degradation. On the contrary, the surface deformations of the GFRP reinforcements of the condition specimens exhibited better characteristics compared to that of BFRP reinforcements, such as adequate shear strength and rigidity. These characteristics enabled the rebar to provide sufficient lateral confinement through rib bearings. As a result, the deformation of the GFRP rebar was not completely sheared off or crushed transversally by the bearing force exerted by the concrete; nevertheless, the overall shape of the rebar could be identified. However, when the conditioned GFRP-reinforced specimens were tested after passing a million cycles of loading, the surface of the GFRP rebar sheared off totally, as it is clear in Figure 13b in compared to Figure 12b.

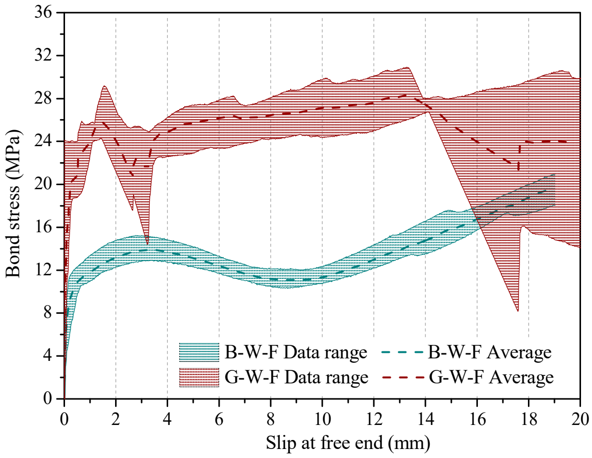

(**a**)

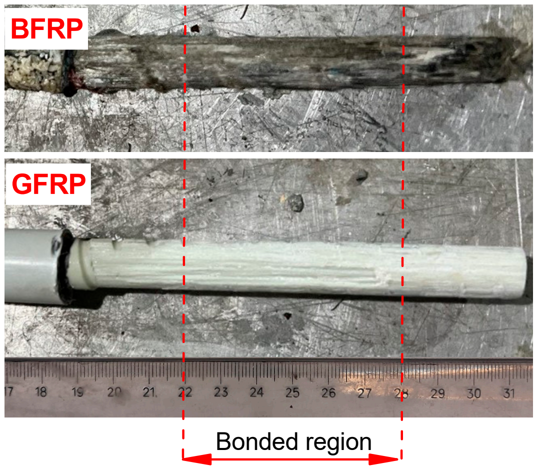

(**b**)

Figure 13. **(a)** Bond behavior of BFRP-reinforced specimens versus that of GFRP-reinforced specimens immerged in simulated seawater, under fatigue loading regime, and (**b**) the condition of the rebars after testing the specimens.

7.5. Modes of Failure

Failure modes of all the tested specimens are reported in Table 4. The specimens subjected to static loading demonstrated a common failure pattern characterized by pull-out (slip), irrespective of the specific type of FRP reinforcement used and the environmental conditions applied. For the tested specimens, namely G-D-S, G-W-S, B-D-S, and B-W-S, no instances of concrete splitting failure were noted. This absence of splitting failure can be attributed to the ample concrete covering provided and the presence of fibers within the concrete, which exert supplementary confining pressure. There were only two exceptions, where one of the B-D-S specimens and one G-W-S specimen exhibited a different behavior.

In contrast, when comparing the failure modes of the specimens subjected to static loading versus fatigue loading, there was a noticeable shift in failure patterns. In fact, the load-slip behavior became more brittle after being subjected to fatigue loading. This shift was observed in most of the control specimens, especially in the case of the G-D-F series, transitioning from pull-out failure to concrete splitting. A similar finding was reported in the research by Wang and Belarbi [28], focusing on the pull-out behavior of GFRP rebar embedded in fiber-reinforced concrete. When the splitting failure occurs, the concrete block is observed to fracture into two or three pieces during the pull-out process, with minimal slippage at the free end of the rebars. This phenomenon primarily results from the inadequate constraint of the rebars by the concrete protective layer, causing the tangential tensile stress due to radial forces to surpass the concrete's splitting tensile strength.

During the splitting mode of failure, micro-cracks initially appear at the rebar–concrete interface, gradually propagating to the outer surface of the concrete block as loading continues, and finally developing into longitudinal splitting cracks. Consequently, specimen failure exhibits a brittle and abrupt nature, leading to a significant reduction in bond stress.

However, as previously mentioned, immersing the specimens reinforced with BFRP in seawater led to deterioration, particularly on the external surface of the BFRP reinforcement. Consequently, bond strength suffered. This deterioration caused the failure mode of the B-W-F specimens to revert to the pull-out mode as shown in Figure 14. In fact, by long-time immersing BFRP-reinforced concrete in seawater, Cl^- ions attempt to penetrate the surface of the basalt fibers and react with pre-existing Fe^{2+} ions within the fibers. The expansion of $Fe_2O_3{\cdot}nH_2O$, resulting from water absorption, further contributes to the de-bonding between the resin and fibers as a byproduct of the aforementioned reaction [34]. The Seawater exposure can lead to damage, particularly on the outer surface of the reinforcement, resulting in a reduced contact area of the FRP with concrete, and deterioration of bond strength.

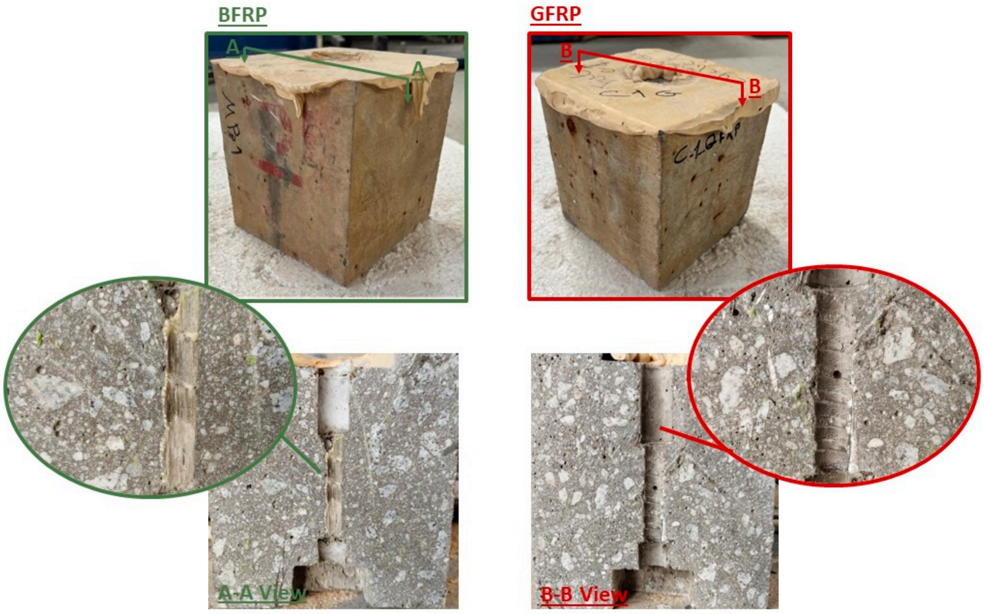

(**a**) (**b**)

Figure 14. Common failure modes observed by conducting the pull-out test on specimens reinforced with (**a**) BFRP and (**b**) GFRP after prolonged exposure to seawater.

8. Prediction of Long-Term Bond-Strength Retention

Evaluating the bond strength between FRP rebars and concrete after prolonged exposure to adverse environments is of paramount significance as it directly influences robust structural safety over the intended service life. By comprehensively examining the repercussions of these challenging conditions over an extended duration, it becomes possible to optimize the bond behavior of the structures. This enhancement not only serves to mitigate potential risks but also ensures the long-lasting durability of the structural elements. In the present section, the prediction of long-term bond-strength retention for the basalt- and glass-FRP-reinforced specimens was conducted using the approach outlined in [34].

The process for predicting long-term bond strength retention is composed of the five following stages: (i) first of all, it is essential to establish degradation curves for the bond strength of the FRP-reinforced specimens subjected to a marine environment. This can be achieved by fitting a linear equation (power equation) onto a logarithmic scale. It is necessary to exclude any lines that demonstrate an upward trend from the analysis. This step is taken because upward trends have the potential to produce unrealistic values, thereby compromising the assurance of the predicted bond strength's safety [13]; (ii) then, the slope of each valid degradation curve, represented as "m", should be determined in the second step; (iii) in the next step (third step), the standard reduction in percentage per decade, R_{10}, which is caused by environmental impact should be evaluated using Equation (3).

$$R_{10} = 100 - (10^m \times 100) \quad [\%] \tag{3}$$

This reduction can be extrapolated from each individual degradation line (*iv*) in the sixth step, the influence term "n" is calculated using Equation (4):

$$n = n_{mo} + n_T + n_{SL} \tag{4}$$

where n_{mo}, n_T, and n_{SL}, respectively, represent the impact of moisture condition, temperature, and desired service life as identified in Table 5; (v) finally, the bond strength should be diminished by an amount denoted as '$\eta_{env,b}$', that can be evaluated based on the following equation:

$$\eta_{env,b} = 1/[(100 - R_{10})/100]^n \quad (5)$$

Table 5. Degradation terms [13].

Degradation Term	Criterion	Value
n_{mo}—Moisture	Dry (50%)	−1
	Moist (80%)	0
	Saturated (100%)	1
n_T—Mean annual temperature (MAT)	<5 °C	−0.5
	>5 °C to <15 °C	0
	>15 °C to <25 °C	0.5
	>25 °C to <35 °C	1
n_{SL}—Desired service-life	1 year	1
	10 years	2
	50 years	2.7
	100 years	3

By following the outlined procedure depicted in the flowchart in Figure 15, and elaborated upon earlier, the retained bond strength percentage obtained through testing specimens exposed to varying durations of seawater saturation (i.e., 24 h and 17,520 h), was subjected to a linear fit on a logarithmic scale as shown in Figure 16a. Notably, instances of retentions exceeding 100%, signifying bond strengths higher in aged specimens than in control specimens, resulted in an upward trend observed in the fitting related to GFRP-reinforced specimens tested under fatigue loading (Figure 16a). Consequently, in accordance with the procedure delineated above for prediction of the long-term bond strength, these results were excluded from the analysis to ensure the maintenance of safety considerations. The slopes of the remaining curves, m, were computed and presented in Table 6. For the specimens conditioned for the duration of 24 months at 23 °C simulated seawater, the environmental influence parameter, R_{10}, exhibited different values of 18.49% for the BFRP-reinforced specimens tested under the static loading regime, and 22.44% for BFRP-reinforced specimens tested under fatigue cycles of loading. The R_{10} was calculated as 1.6% for those specimens reinforced using GFRP rebars and tested using static load. In this study, a fixed service life of 50 years was considered for the prediction of the retained bond strength. By using the calculated values of R_{10} as well as the established values of n based on Table 5, the bond-strength retentions after 50 years were predicted as: 42.40% and 34.36% for the BFRP-reinforced specimens tested under static and fatigue loading regimes, respectively, and 93.40% for GFRP-reinforced specimens tested monotonically. Based on the predicted bond strength of specimens following 50 years of saturation in seawater, it is evident that favorable outcomes were achieved when employing GFRP rebars to reinforce offshore structures. Nonetheless, the utilization of BFRP reinforcements demands heightened prudence of design for structures operating within offshore environments, particularly under conditions involving cyclic loading.

This study involves a comparative analysis between the retained tensile strength in BFRP rebars and the bond strength between BFRP rebars and concrete, by considering the results obtained in this study and the findings from Serbescu et al. [35]. Serbescu et al. [35] employed the fib Bulletin 40 [20] methodology to predict the preservation of tensile strength in BFRP rebars after a century of service. To enable a direct and meaningful comparison, predictions were also made for the retention of bond strength over the same 100-year period (Figure 16). The outcome revealed a bond strength retention rate of 41% (for B-W-S after 100 years), accounting for the saturated moisture environment and Mean

Annual Temperature (MAT) ranging from 15 °C to 25 °C. In comparison, Serbescu et al. [35] demonstrated a tensile strength retention of 62% under saturated conditions at 20 °C. These depicted outcomes can be observed in Figure 16b. As expected, the retention of tensile strength in the rebars surpasses that of bond strength. However, additional investigations are warranted to ascertain whether a correlation exists between the preservation of tensile strength and bond strength in FRP rebars. Moreover, there is a need to elucidate how these dual deteriorations should be integrated to derive accurate and dependable forecasts regarding the performance of FRP reinforcing rebars.

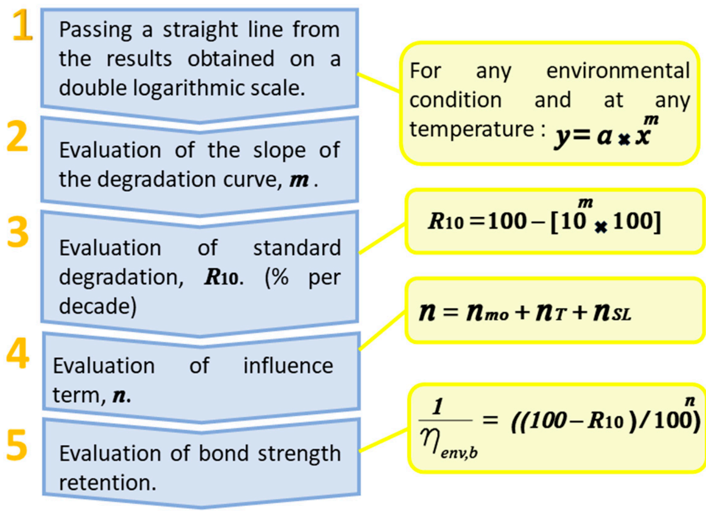

Figure 15. Flowchart of evaluation of bond strength retention based on fib bulletin 40 [34] method.

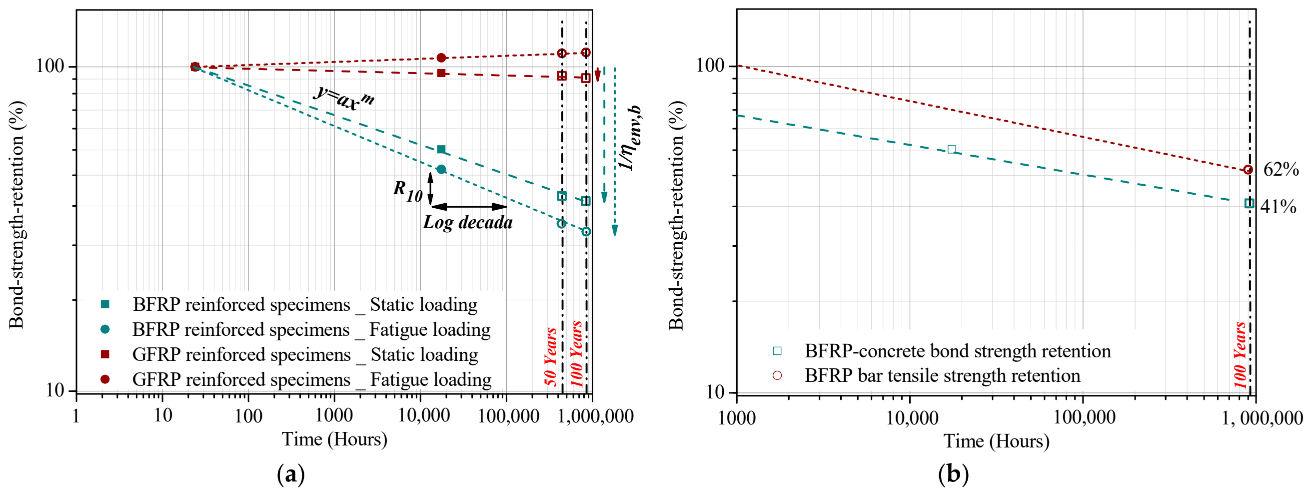

Figure 16. (**a**) Prediction of bond strength retention for 50 years of service life according to fib bulletin 40 [34] method, and (**b**) comparison between BFRP rebar tensile strength retention and bond strength retention for 100 years of service life.

Table 6. Bond strength retention prediction after 50 years of service life [34].

Specimen ID	m (-)	R_{10} (%)	n (50 Years)	$\eta_{env,b}$ (-)	$1/\eta_{env,b}$ (%)
GFRP-reinforced specimens, static loading	−0.007	1.60	4.2	1.07	93.40
GFRP-reinforced specimens, static loading	−0.088	18.49	4.2	2.36	42.40
GFRP-reinforced specimens, fatigue loading	−0.110	22.43	4.2	2.91	34.36

9. Conclusions

This study sought to offer significant insights into the behavior of the BFRP-FRSCC bond under prolonged exposure to challenging environmental conditions. This investigation was conducted with a keen awareness of their significance in informing structural design practices. From the comprehensive analysis of test outcomes and the ensuing discussions in this research, the following key conclusions can be established:

(*i*) Bond performance of the specimens at normal conditions:

- Compared to the specimens reinforced with GFRP, those incorporating BFRP rebars exhibited consistently higher bond strength across all loading phases at normal (laboratory) conditions.
- The BFRP rebar achieved a noteworthy 17% increase in average bond strength, Av. τ_{max}, likely attributed to the ribbed and spiral surface of the BFRP material, which facilitated the formation of a robust 3D resistance mechanism along the length of the rebar. Thus, the predominance of peeling action on the surface of BFRP was mitigated, by propagation of cracks around the bond region, governing the stress–slip relationship.
- Fatigue loading can improve the bond behavior of the FRP-reinforced concrete elements, particularly in the post-peak phase. Under normal conditions, BFRP-reinforced specimens showed a 10% enhancement in their post-peak bond response corresponding to 20 mm free end slip of BFRP rebars, while GFRP-reinforced specimens exhibited a more substantial improvement of 45%. Notably, this alteration was accompanied by a transition in the mode of failure from slipping the rebar, i.e., the pull-out failure, to splitting of the concrete.

(*ii*) Bond performance of the specimens after prolonged seawater exposure:

- Prolonged exposure to seawater significantly weakened the bond slip (τ-s) response of BFRP-reinforced specimens. In comparison to unconditioned specimens, a substantial reduction of 55.7% and 49% was observed in the maximum bond strength of the conditioned BFRP-reinforced ones under static and fatigue loading regimes, respectively.
- Compared to unconditioned specimens, the residual bond strength of the conditioned BFRP-reinforced specimens, with a 20 mm free end slip, decreased by 33.5% and 18.8% under quasi-static and fatigue loading, respectively. In contrast, GFRP-reinforced specimens showed nearly identical bond strength to their corresponding control specimens after immersion in seawater.
- Out of all the different types of pull-out specimens, the minimum bond strength (equal to 12.4 MPa), was observed in the case of the B-W-S series, that can be attributed to moisture absorption in the BFRP due to long-term immersion in seawater. The bond strength in these specimens still fulfilled the requirements of the bond strength outlined in ACI 440.6 M (>9.6 MPa) [36]. Conversely, the B-D-F specimens, tested under normal conditions and in a fatigue loading regime, achieved the highest bond strength at 27.30 MPa, by surpassing the performance of the B-D-S specimens by 10% in the post-peak phase.

(*iii*) Possibilities in designing durable offshore structures:

- The applied concrete reinforced with hybrid RTSF and ISF stands out as a promising solution for constructing offshore structural elements of longer service life. In addition to the beneficial fiber-bridging effect that governs the post-peak properties of the bond response by its bridging effect, the developed FRSCC also demonstrates remarkable resistance to strength deterioration caused by corrosion.

Given that the conclusions drawn in the present study were derived from an examination of specific FRP rebars, it is imperative to underscore the need for further research. This subsequent research should delve into bond durability issues by exploring the influence of diverse concrete strengths, varying hush environments, and extended exposure durations. Furthermore, there are no firmly established correlation factors yet that reliably connect the outcomes of accelerated aging procedures with aging tests by natural exposure to bond behavior studies. Future research efforts should aim to enhance our understanding and predictive capabilities by addressing these challenges and pursuing a more robust correlation between accelerated aging tests and real-world environmental exposures.

Author Contributions: Conceptualization, F.S.; Methodology, F.S. and A.E.-B.; Formal analysis, F.S.; Investigation, F.S., A.E.-B., K.H. and I.F.C.; Resources, F.S., J.M.O. and R.L.R.; Writing—original draft, F.S.; Writing—review & editing, A.E.-B., I.F.C., J.M.O. and R.L.R.; Supervision, F.S., J.M.O. and R.L.R.; Project administration, F.S.; Funding acquisition, F.S., J.M.O. and R.L.R. All authors have read and agreed to the published version of the manuscript.

Funding: The authors express their gratitude for the support provided by the FLOATIDE project, reference POCI-01-0145-FEDER-028112, co-financed by the European Regional Development Fund (ERDF) under Portugal 2020, through the Operational Program for Competitiveness and Internationalization (COMPETE 2020), as well as by the Fundação para a Ciência e a Tecnologia—FCT I.P. (National Agency for Science and Technology). The first author also acknowledges the Scientific Employment funding, No. CEECIND/01627/2017, provided by FCT I.P. IFC also thanks the FCT, and acknowledges the FCT distinction attributed to IFC under the Estímulo ao Emprego Científico program (2021.01969.CEECIND).

Institutional Review Board Statement: Not applicable.

Informed Consent Statement: Not applicable.

Data Availability Statement: All necessary data supporting the reported results have been meticulously included in the manuscript. However, for specific requests or inquiries regarding the data, interested parties are welcome to contact the corresponding author via email. We are committed to transparency and open communication, and we will promptly address any data-related queries.

Acknowledgments: The authors express their appreciation for the collaboration extended by the following companies: Schöck Bauteile GmbH; Recipneu—Empresa Nacional De Reciclagem De Pneus, Lda; BASF Portuguesa S.A.; Secil; RENECAL—Reciclado De Neumáticos De Castilla Y León S.L.; Celtejo/ALTRI group; Sika Portugal—Produtos Construção e Indústria S.A.; PARAPEDRA; MOTA-ENGIL, and Unibetão.

Conflicts of Interest: The authors declare no conflict of interest.

References

1. Soltanzadeh, F.; Edalat Behbahani, A.; Hosseinmostofi, K.; Teixeira, C.A. Assessment of the sustainability of fibre-reinforced concrete by considering both environmental and mechanical properties. *Sustainability* **2022**, *14*, 6347. [CrossRef]
2. Zamanzadeh, Z.; Lourenço, L.; Barros, J. Recycled Steel Fibre Reinforced Concrete failing in bending and in shear. *Constr. Build. Mater.* **2015**, *85*, 195–207. [CrossRef]
3. Soltanzadeh, F.; Edalat-Behbahani, A.; Barros, J.; Mazaheripour, H. Effect of fiber dosage and prestress level on shear behavior of hybrid GFRP-steel reinforced concrete I-shape beams without stirrups. *Compos. Part B Eng.* **2016**, *102*, 57–77. [CrossRef]
4. Uomoto, T. Use of fiber-reinforced polymer composites as reinforcing material for concrete. *J. Mater. Civil. Eng.* **2002**, *14*, 191–209. [CrossRef]
5. Tao, Y.; Hadigheh, S.A.; Wei, Y. Recycling of glass fibre reinforced polymer (GFRP) composite wastes in concrete: A critical review and cost benefit analysis. *Structures* **2023**, *53*, 1540–1556. [CrossRef]
6. Lu, Z.; Li, W.; Zeng, X.; Pan, Y. Durability of BFRP bars and BFRP reinforced seawater sea-sand concrete beams immersed in water and simulated seawater. *Constr. Build. Mater.* **2023**, *363*, 129845. [CrossRef]
7. Abed, F.; Alhafiz, A.R.J.C.S. Effect of basalt fibers on the flexural behavior of concrete beams reinforced with BFRP bars. *Compos. Struct.* **2019**, *215*, 23–34. [CrossRef]
8. Hua, Y.; Yin, S.; Feng, L. Bearing behavior and serviceability evaluation of seawater sea-sand concrete beams reinforced with BFRP bars. *Constr. Build. Mater.* **2020**, *243*, 118294. [CrossRef]
9. Soltanzadeh, F.; Edalat Behbahani, A.; Pereira, E.N.B. Bond behavior of recycled tyre steel fiber reinforced concrete and basalt fiber-reinforced polymer bars under static and fatigue loading conditions. *J. Build. Eng.* **2023**, *70*, 106291. [CrossRef]
10. Abdallah, M.; Al Mahmoud, F.; Khalil, N.; Khelil, A. Effect of the strengthening patterns on the flexural performance of RC continuous beams using FRP reinforcements. *Eng. Struct.* **2023**, *280*, 115657. [CrossRef]
11. Dong, Z.; Wu, G.; Zhao, X.-L.; Zhu, H.; Lian, J.-L. Durability test on the flexural performance of seawater sea-sand concrete beams completely reinforced with FRP bars. *Constr. Build. Mater.* **2018**, *192*, 671–682. [CrossRef]
12. Zhang, B.; Wang, W.; Yang, Z.; Zhu, H. Understanding the bond performance between BFRP bars and alkali-activated seawater coral aggregate concrete under marine environments. *Eng. Struct.* **2023**, *288*, 116228. [CrossRef]

13. Nepomuceno, E.; Sena-Cruz, J.; Correia, L.; D'Antino, T. Review on the bond behavior and durability of FRP bars to concrete. *Constr. Build. Mater.* **2021**, *287*, 123042. [CrossRef]
14. Guo, X.; Jin, Z.; Xiong, C.; Sun, T.; Li, N.; Yu, Y.; Zhang, X. Deterioration of mechanical properties of basalt/carbon hybrid FRP bars in SWSC under seawater corrosive environment, Construct. *Build. Mater.* **2022**, *317*, 125979. [CrossRef]
15. Taha, A.; Alnahhal, W.; Alnuaimi, N. Bond durability of basalt FRP bars to fiber reinforced concrete in a saline environment. *J. Compos. Struct.* **2020**, *243*, 112277. [CrossRef]
16. Hallonet, A.; Ferrier, E.; Michel, L.; Benmokrane, B. Durability and tensile characterization of wet lay-up flax/epoxy composites used for external strengthening of RC structures. *Constr. Build. Mater.* **2019**, *205*, 679–698. [CrossRef]
17. *BS EN 12350-8*; Testing Fresh Concrete, Self-compacting Concrete. Slump-flow Test. BSI: London, UK, 2010.
18. *BS EN 12390-13*; Testing Hardened Concrete—Part 13: Determination of Secant Modulus of Elasticity in Compression. BSI: London, UK, 2014.
19. *ASTM C39/C39M-14*; Standard Test Method for Compressive Strength of Cylindrical Concrete Specimens. American Society of Testing Materials: Conshohocken, PA, USA, 2014.
20. FIB-Fédération Internationale du Béton. *Fib Bulletin 40, FRP Reinforcement in RC Structures*; FIB-Fédération Internationale du Béton: Lausanne, Switzerland, 2007.
21. Frigione, M.; Rodríguez-Prieto, A. Can Accelerated Aging Procedures Predict the Long Term Behavior of Polymers Exposed to Different Environments? *Polymers* **2021**, *13*, 2688. [CrossRef] [PubMed]
22. Zhang, K.; Zhang, Q.; Xiao, J. Durability of FRP bars and FRP bar reinforced seawater sea sand concrete structures in marine environments. *J. Constr. Build. Mater.* **2022**, *350*, 128898. [CrossRef]
23. Guo, J.; Zhan, L.; Ma, B.; Zhang, D.; Fan, Y.; Yao, S.; Feng, J. A review on failure mechanism and mechanical performance improvement of FRP-metal adhesive joints under different temperature-humidity. *Thin-Walled Struct.* **2023**, *188*, 110788. [CrossRef]
24. Zeng, J.J.; Zhuge, Y.; Liang, S.D.; Bai, Y.L.; Liao, J.J.; Zhang, L. Durability assessment of PEN/PETFRP composites based on accelerated aging in alkaline solution/seawater with different temperatures. *J. Constr. Build. Mater.* **2022**, *327*, 126992. [CrossRef]
25. RILEM TC 162-TDF, Bending test. *Mater. Struct.* **2002**, *35*, 579–582. [CrossRef]
26. *ASTM D1141-98*; "Standard Practice for the Preparation of Substitute Ocean Water". American Society of Testing Materials: Conshohocken, PA, USA,, 2004.
27. Chu, S.H.; Kwan, A.K.H. A new method for pull-out test of reinforcing bars in plain and fibre reinforced concrete. *Eng. Struct.* **2018**, *164*, 82–91. [CrossRef]
28. Wang, H.; Belarbi, A. Static and fatigue bond characteristics of FRP rebars embedded in fiber-reinforced concrete. *J. Compos. Mater.* **2010**, *44*, 1605–1622. [CrossRef]
29. Frazão, C.; Diaz, B.; Barros, J.; Bogas, J.A.; Toptan, F. An experimental study on the corrosion susceptibility of Recycled Steel Fibre Reinforced Concrete. *Cem. Concr. Compos.* **2019**, *96*, 138–153. [CrossRef]
30. Ding, Y.; Ning, X.; Zhang, Y.; Pacheco-Torgal, F.; Aguiar, J.B. Fibres for enhancing of the bond capacity between GFRP rebar and concrete. *Construct. Build. Mater.* **2014**, *51*, 303–312. [CrossRef]
31. Lei, W.; Yadong, M.; Haibo, L.; Shuang, C.; Wei, L. Bond properties between FRP bars and coral concrete under seawater conditions at, 30, 60 and 80 °C. *Constr. Build. Mater.* **2018**, *162*, 442–449. [CrossRef]
32. Lu, Z.Y.; Xian, G.J.; Li, H. Effects of elevated temperatures on the mechanical properties of basalt fibers and BFRP plates. *Constr. Build. Mater.* **2016**, *127*, 1029–1036. [CrossRef]
33. Wang, Z.; Zhao, X.L.; Xian, G.; Wu, G.; Singh Raman, R.K.; Al- Saadi, S.; Haque, A. Long-term durability of basalt- and glass-fibre reinforced polymer (BFRP/GFRP) bars in seawater and sea sand concrete environment. *Constr. Build. Mater.* **2017**, *139*, 467–489. [CrossRef]
34. Hussain, S.; Khan, M.Z.N.; Khan, H.A. Bond performance of basalt FRP bar against aggressive environment in high-strength concrete with varying bar diameter and bond length. *Constr. Build. Mater.* **2022**, *349*, 128779. [CrossRef]
35. Serbescu, A.; Guadagnini, M.; Pilakoutas, K. Mechanical characterization of basalt FRP rebars and long-term strength predictive model. *J. Compos. Constr.* **2014**, *19*, 04014037. [CrossRef]
36. ACI Committee 440. *Specification for Carbon and Glass Fiber-Reinforced Polymer Bar Materials for Concrete Reinforcement (ACI 440.6M-08)*; American Concrete Institute: Farmington Hills, MI, USA, 2008; p. 6.